UV distributed Bragg reflectors build from porous silicon multilayers

F. Morales CIDS-ICUAP. Benemérita Universidad Autónoma de Puebla, C.P. 72570 Puebla, México

G. García CIDS-ICUAP. Benemérita Universidad Autónoma de Puebla, C.P. 72570 Puebla, México

A. Luna CIDS-ICUAP. Benemérita Universidad Autónoma de Puebla, C.P. 72570 Puebla, México

R. López lorr810813@gmail.com Laboratorio de Investigación y Desarrollo de Materiales Avanzados (LIDMA), Facultad de Química, Universidad Autónoma del Estado de México, Paseo Colón esquina Paseo Tollocan, Toluca Estado de México, 50110, México

E. Rosendo CIDS-ICUAP. Benemérita Universidad Autónoma de Puebla, C.P. 72570 Puebla, México

T. Díaz CIDS-ICUAP. Benemérita Universidad Autónoma de Puebla, C.P. 72570 Puebla, México

H. Juárez CIDS-ICUAP. Benemérita Universidad Autónoma de Puebla, C.P. 72570 Puebla, México

UV Distributed Bragg reflectors were fabricated by a two-step thermal oxidation process over porous silicon multilayers (PS-ML), which were prepared by room-temperature electrochemical anodization of silicon wafers. The optical behavior of the PS-ML before and after oxidation was studied by reflectance measurements. It was observed an UV shift from 430 to 300 nm in the peak of the reflectance spectrum after oxidation of the PS-ML. This was attributed to the presence of silicon oxide over the surface of the silicon filaments. Such oxide also reduced the refractive index of each porous silicon monolayer. The bandgap of the PS-ML was calculated by the Kubelka-Munk approximation, which showed an increase in the bandgap from 3.11 to 4.36 eV after the thermal oxidation process. It was suggested that the observed optical response could opens the possibility of fabrication of UV optoelectronic devices based entirely in the silicon technology.
[DOI: http://dx.doi.org/10.2971/jeos.2015.15016]

Keywords: Porous silicon, thermal oxidation, multilayers, ultraviolet (UV)

1 INTRODUCTION

Porous silicon (PS) is a versatile material with potential application in optical and electronic devices such as light emitting diodes [1, 2], photodetectors [3], gas sensors [4, 5], among others. PS can be considered as a silicon crystal composed by alternating silicon filaments and nano-sized air holes, also called pores. The refractive index (RI) of PS can be modulated in the range of 1.1 to 3.5 by the control of its porosity. This RI modification has allowed the design and fabrication of silicon-based optical devices. Ultra violet (UV)-reflective coatings are the main building-blocks for fabrication of optical devices such as lasers, Fabry-Perot filters, and distributed Bragg reflectors (DBR) [6]–[8]. Recently, M. Liang et al have reported that nanostructured-oxidized PS exhibited a wide band-gap (Eg) [9], which can be useful in fabrication of short-wavelength devices. According to Suemune et al. [10], the pore size must be reduced to less than 2 nm to achieve wide-Eg features. Partially-oxidized PS has greater sensitivity and a lower RI than its non-oxidized counterpart [11, 12]. The DBR can be easily produced by periodically raising and lowering the electrochemical current flowing through highly-doped p-type silicon during anodization. Therefore, both the porosity and the effective RI of each PS layer are mainly determined by the applied current density [13]. If a high/low RI is alternated on each layer of the porous silicon multilayer structure, having an optical thickness of one quarter of the wavelength of the incident light, this wavelength is constructively reflected. Gelloz and coworkers have fabricated DBR with efficient UV response [14]. In their experiments, anodization temperature of silicon wafers was -20 °C and a subsequent water vapor annealing at a pressure of 2.6 MPa was performed on the PS-ML. According to the study authors, these experimental conditions favored the formation of a high quality oxide, which reduced the interfacial defect density in the silicon filaments. In the present work, UV-DBR were fabricated in two steps: first by electrochemical anodization of silicon wafers, and later by oxidation of the obtained PS-ML. The anodization of the silicon wafers was conducted at room-temperature. Thermal oxidation of the PS-ML was carried out in two steps: the first was a pre-oxidation step at 350 °C, and the second one was a high-temperature annealing at 850 °C . Both oxidation steps were conducted at atmospheric pressure. The RI of air, silicon and silicon oxide were calculated to predict the maxima of the re-

Received November 12, 2014; revised ms. received March 01, 2015; published March 21, 2015 ISSN 1990-2573

flectance peak in the UV region [15]. It is suggested that the fabricated UV-DBR would be a suitable candidates for applications in short-wavelength devices since the formed structures are nano-sized PS with wide band-gap [16, 17].

2 EXPERIMENTAL DETAILS

PS-ML were prepared by electrochemical anodization of p-type boron-doped (100) oriented crystalline silicon wafers ($\rho = 0.01 - 0.02\Omega$-cm), which were previously submerged in a 20 % hydrofluoric acid (HF) solution to remove native oxides. The electrochemical etching was carried out in an electrolyte based on HF (40 %) and ethanol (99.6 %), at a volumetric ratio of 1:1. The anodization current density was provided by a computer-controlled power supply (Keithley 2400). The scheme of the experimental setup used to prepare the DBR is shown in Figure 1.The porosity percent and the thickness of the etched samples were measured by the gravimetric method [17]. A current density (J) in the range of 1-140 mA/cm^2 was applied over an area of 1.0 cm^2 of the silicon wafer. Figure 2 shows the (a) porosity (%), and (b) the etching rate as a function of J. The RI of each PS monolayer was calculated by the Bruggeman's model [18], which uses an effective medium approximation. The Bruggeman's approximation has proved to be a suitable model to calculate the RI related to porosity (Eq. (1)):

$$p\frac{(n_p^2 - n_{PS}^2)}{(n_p^2 + 2n_{PS}^2)} + (1-p)\frac{(n_f^2 - n_{PS}^2)}{n_f^2 - 2n_{PS}^2} = 0 \qquad (1)$$

Where p is the porosity of each PS monolayer, n_p is the RI of air, which is the material filling out the pores (taking n_p = 1 in all cases); n_f is the RI of silicon filaments and n_{PS} is the resulting RI of the PS monolayer. The fabricated DBR consists of a stack of PS layers with alternated RI values and a central wavelength of 370 nm (with ten periods). A period consists of two layers with high (n_H) and low (n_L) RI. We have taken into account the function $n_i(\lambda)$ (where i = H,L) and the condition $n_i d_i = \lambda_0/4$ for the thicknesses d_i. It has been reported that under similar hydrofluoric acid concentration during anodization and p-type doping level in silicon, the average pore size was about 10 nm in diameter [9], [19]–[21]. Thus, before oxidation the structure size of the pore can be considered as mesoporous silicon. Since oxidation of silicon at high temperatures can induce uncontrolled changes in the porous structure and an unstable silicon oxide could be formed, oxidation of the PS-ML was performed (oxygen gas, flowed at a rate of 10 sccm) in two steps: first, in the pre-oxidation step, the samples were oxidized at 350 °C for 15 min to stabilize the porous structure, and prevent coarsening during the following oxidation step, which could result in poor reproducibility [22, 23]. The second oxidation step was performed at 850 °C for 10 min to complete the oxidation of silicon, which should not exceed the 44 % of its thickness [24]. The reflectance measurements were performed with an UV-vis spectrometer (Thermo Scientific Evolution 600).

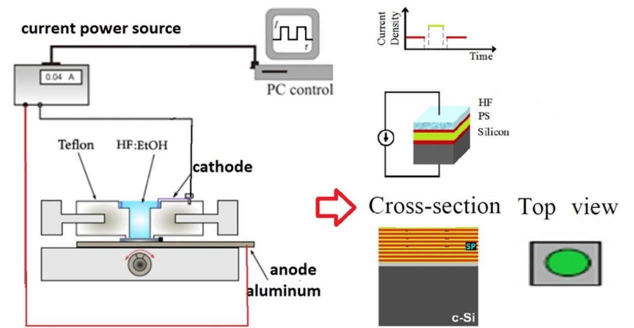

FIG. 1 On the left it is show the electrochemical etching setup and the components of the etching cell. On the right the scheme of porous silicon multilayer stack formation is shown.

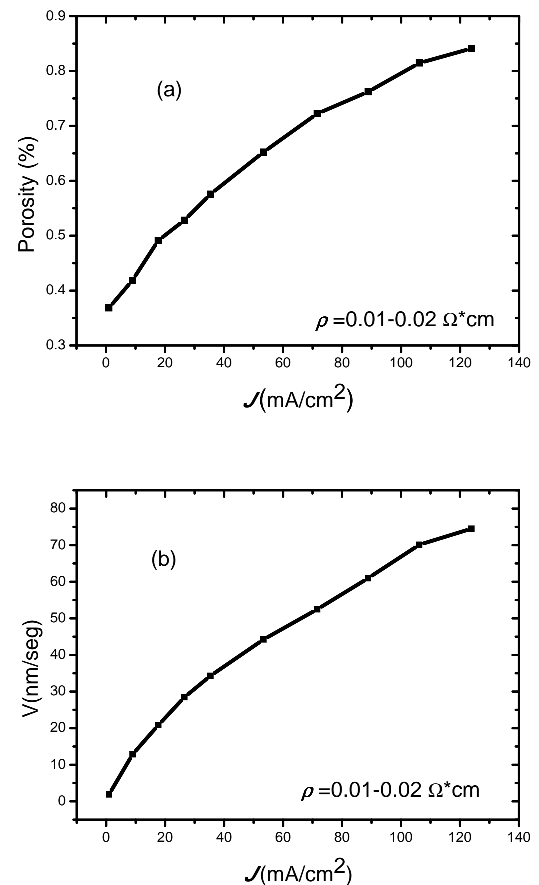

FIG. 2 a) Porosity and b) etching rate as a function of the applied current density.

3 RESULTS

Table 1 shows the optical parameters, thicknesses (d) and porosities (P %), before thermal oxidation the PS-ML. The aim of this study was to achieve UV features in the fabricated DBR. Thus, for anodization of the silicon wafers, the refractive index and the thickness of each PS monolayer was calculated to reach a wavelength of 370 nm.

Sample	λ (nm)	n_H	n_L	d (nm) H	d (nm) L	P% H	P% L
PS-ML before oxidation	370	4.41	1.38	24.53	74	42	82

TABLE 1 DBR parameters calculated for the PS-ML before oxidation.

Figure 3 shows the reflectance spectra for the PS-ML before and after thermal oxidation. The reflectance spectrum of PS-ML before thermal oxidation (Figure 3(a)), exhibits a strongest peak at a wavelength of about 425 nm, which is very close to the calculated by the Bruggemman's aproximation. After oxidation (Figure 3(b)), the peak shifts to 300 nm in the near-UV region. This effect is known as "blue-shift", and is commonly observed in PS-ML annealed in oxygen-rich atmospheres. However, it is important to note that this shift is usually observed into the visible light spectrum [25]. The lack of reports of silicon-based materials with performance in the UV region is due to the loss of the efficiency of the reflectance response in short wavelengths [26]–[28]. It can also be seen that the bandwidth of the reflectance peak before and after oxidation of the PS-ML is smaller than that of multilayer structures deposited by epitaxial techniques [29]. Since each layer prepared by electrochemical anodization of silicon has a porous structure, it is expected that this porous media will lead to significant scattering at short wavelengths, and consequently the bandwidth will be reduced. Moreover, the maxima of the reflectance peak for the PS-ML before and after oxidation have similar percentage of reflectance, which could be evidence that the crystalline silicon absorption at short wavelengths was almost negligible. It is known that the fabrication of optical UV silicon-based devices has been a difficult task since silicon absorption increases at short wavelengths. In Figure 3, it is also observed that both the bandwidth and the reflectance percent of the PS-ML was decreased after oxidation due to dispersion effects at short wavelengths. However, the optical losses of the PS monolayers were reduced by the silicon oxide formed on the surface of the silicon filaments. This can be attributed to the null contribution of the imaginary part of the RI of silicon oxide [30]. Thus, silicon oxide can be regarded as a material with low optical losses at short wavelengths. It has also been demonstrated that the optimal conditions for efficient reflectance in the UV was favored by the formation of a high quality oxide over the silicon filaments [14].

In Table 2, the optical parameters, thicknesses (d) and porosities (P %) for the oxidized PS-ML are shown. The comparison between Table 1 and 2 reveals that a decrease in the RI was obtained after oxidation of the PS-ML. Such decrease can be understood if it is considered that during thermal oxidation, the silicon structure is replaced by silicon oxide, which has a RI lower than that of silicon. This oxidation decreases the RI value of the PS structure and consequently the optical thickness of each PS monolayer. However, due to the self-limiting nature of the thermal oxidation, only a fraction of silicon was transformed into silicon oxide.

It is known that during oxidation of crystalline silicon, there is a volume expansion with the addition of oxygen. This expansion occurs because the density of silicon oxide is slightly less than that of crystalline silicon. With the use of densities and molecular weights of crystalline silicon and silicon oxide respectively, it is possible to calculate the volume expansion [24]. The growth of an oxide of thickness x will consume a layer of silicon of about $0.44x$ thick. It can thus be assumed that the oxidized PS structure is composed by three components: crystalline silicon, silicon oxide and air [31]. The refractive index (n_{pso}) of the oxidized PS-ML was calculated using a model that considers the three media [15]. The equation that supports that model is as follows (Eq. (2)):

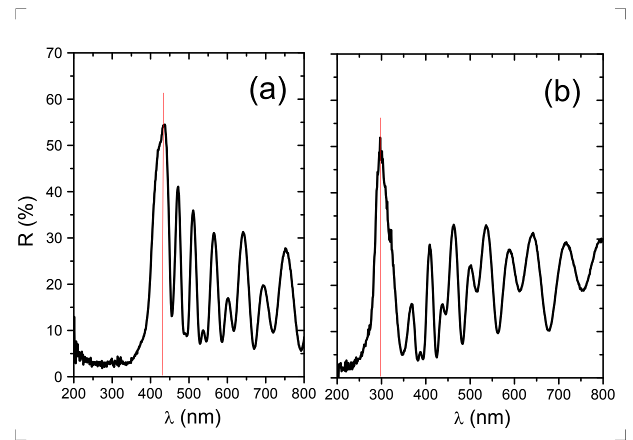

FIG. 3 Reflectance spectra of the PS-ML: (a) as formed, and (b) after oxidation.

$$n_{pso}(\lambda) = p * n_{air}(\lambda) + (1-p)[f * n_{si}(\lambda) + (1-f) * n_{siO2}(\lambda)] \quad (2)$$

where, p is the fraction of air (porosity) and f is the fraction of crystalline silicon that was not oxidized. The values of the refractive index of crystalline silicon and silicon oxide have been previously reported in the literature [30]. The results of the n_{pso} (λ) of oxidized PS-ML plotted versus selected PS porosities (Figure 4), show not only that the n_{pso} (λ) gradually decreases as the P (%) increases but also that the RI is found in wavelengths less than 400 nm, which confirms the same optical behavior as the non-oxidized PS-ML structure.

Sample	λ (nm)	n_H	n_L	d (nm) H	d (nm) L	P% H	P% L
Oxidized PS-ML	300	3.21	1.20	23.36	62.5	33	65

TABLE 2 DBR parameters calculated for the PS-ML after thermal oxidation.

The change in the RI of the oxidized PS-ML can be understood as a result of reduction in the pore size. The surface oxide layer increases the volume occupied by the solid base during oxidation, i.e. decreases the porosity percent. According to reports on preparation of PS monolayers, the RI is reduced by the increase in the oxidation temperature, approaching to the RI of the silicon oxide at temperatures close to 800 °C [31]. However, it is known that in most oxidation processes, the average porosity reduction is about of twenty percent. The optical band gap energy (Eg) of the PS-ML was calculated by the Kubelka-Munk approximation (Eq. (3)), in order to confirm the shift on the optical behavior of the DBR [32]:

$$[F(R_\infty)hv]^2 = C(hv - E_g) \quad (3)$$

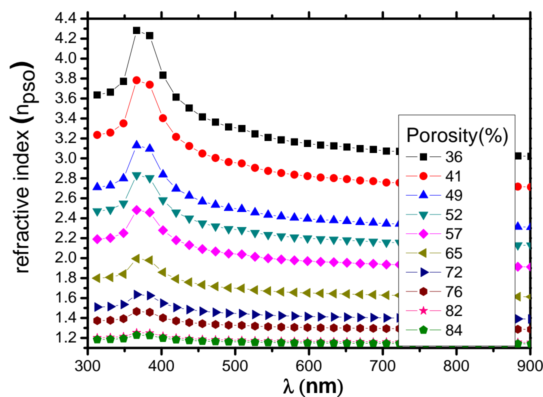

FIG. 4 Refractive index as a function of wavelength, for several porosity percents.

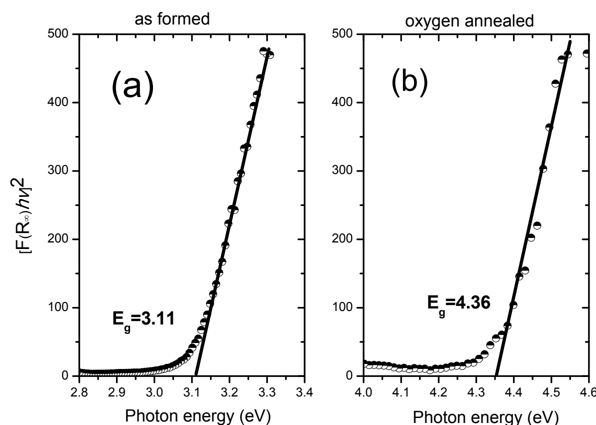

FIG. 5 Reflectance spectra of the PS-ML after Kubelka-Munk treatment: (a) as formed, (b) after oxidation.

Where, $F(R_\infty)$ is the so-called remission or Kubelka-Munk function, $h\nu$ is the photon energy and C is a proportionality constant. The Kubelka-Munk model is based on several assumptions: 1.The medium (sample) is modeled as a plane layer of finite thickness, but infinite width and length (infinite sheet approximation), so there are no boundary effects. 2. A perfectly diffuse and homogeneous illumination impinges on the surface. 3.The only interactions of light with the medium are scattering and absorption; polarization and spontaneous emission (fluorescence) are ignored. 4. The medium is considered isotropic and homogeneous, containing optical heterogeneities (small compared to the thickness of the layer) able to disperse light [21]. The reflectance spectra of the PS-ML after Kubelka-Munk treatment are shown in Figure 5. The intersection between the linear fit and the photon energy axis gives the E_g value. It was found that the thermal oxidation performed to the PS-ML increased the E_g from 3.11 (Figure 5(a)) to 4.36 eV (Figure 5(b)).

There are scarce reports on the fabrication of PS-ML with efficient response in the UV region. In Table 3, comparative experimental and optical data of the DBR fabricated in this work and those corresponding to Gelloz and coworkers [14], are shown. Gelloz suggested that high anodization temperature leads to a decrease in the porosity and consequently in an increase in the RI, which could resulted in a red-shift. Our results (Figure 3) revealed that a well-defined peak of reflectance was obtained under anodization performed at room-temperature. In general, Gelloz and coworkers obtained a high stability of the DBR in their low-temperature anodization and high-pressure annealing experiments, which was manifested in high transparency of the DBR. However, in the present work it was observed that the room-temperature anodization of the silicon wafers and controlled two-step oxidation of the PS-ML was an efficient way to achieve UV features in the fabricated DBR.

Parameter		fabricated DBR	DBR Gelloz
	HF concentration (volume)	1:1	1:1
	Current density	10-120 mA-cm^2	5-150 mA-cm^2
	Periods	10	10
$n_H - n_L$:	Before oxidation	4.41-1.38	–
	After oxidation	3.21-1.20	–
	Temperature	Room temperature	-20°C
	Wafer resistivity (p-type doping)	0.01-0.02 Ω-cm	4 Ω-cm
	Temperature, pressure and time during oxidation	First step: 350 °C, 15 min Second step: 850 °C, 10 min Atmospheric pressure, dry oxidation	260 °C, 3 Hrs, High-pressure 1.3-2.6 MPa, water vapor annealing
λ_0	Before oxidation	435 nm	500 nm
	After oxidation	300 nm	335 nm
Porosity	Before oxidation	42-82 %	–
	After oxidation	33-65 %	–
Thickness	Before oxidation	24.5-74 nm	–
	After oxidation	23.3-62.5 nm	–
Eg	Before oxidation	3.11 eV	–
	After oxidation	4.36 eV	–

TABLE 3 Comparative experimental and optical data of the DBR prepared in this work and those corresponding to Gelloz and coworkers.

4 CONCLUSIONS

PS-ML were integrated in a structure known as Distributed Bragg Reflectors.Thermal oxidation performed on the porous silicon multilayers improved its optical behavior over time, modifying the RI of each layer of the PS structure. The UV shift observed in the peak of reflectance spectra was introduced by the deviation in the RI of the PS structure after oxidation. The increase in the optical band gap of the PS-ML after oxidation was confirmed by the Kubelka-Munk approximation. It is suggested that the fabricated PS-ML structures could be used in the design of efficient UV-DBR based only in the silicon technology.

References

[1] Z. C. Feng, and R. Tsu, *Porous Silicon* (World Scientific, Singapore, 1994).

[2] L. Pavesi, R. Guardini, and C. Mazzoleni, "Porous silicon resonant cavity light emitting diodes," Solid State Commun. **97**, 1051 (1996).

[3] V. Torres-Costa, R. J. Martín-Palma, and J. M. Martínez, "All-silicon color-sensitive photodetectors in the visible," Mat. Sci. Eng. C **27**, 954 (2007).

[4] L. Z. Yu, and C. R. Wie, "Fabrication of MSM photoconductor on porous Si using micromachined silicon mask," Electron. Lett. **28**, 911 (1992).

[5] A. M. Rossi, and H. G. Bohn, "Photodetectors from Porous Silicon," Phys. Status Solidi **202**, 1644 (2005).

[6] M. Grau, N. T. Nguyen, A. Straboni, and M. Lemiti, "Structural and optical propeties of Annealend Porous Silicon Bragg Reflector for Thin-Film Crystalline Silicon Solar Cells," Eur. Mat. Res. **10**, 8 (2011).

[7] V. Torres-Costa, R. J. Martín-Palma, and J. M. Martínez-Duart, "Optical characterization of porous silicon films and multilayer filters," Appl. Phys. A-Mater. **79**, 1919 (2004).

[8] E. Lorenzo, C. J. Oton, N. E. Capuj, M. Ghulinyan, D. Navarro, Z. Gaburro, and L. Pavesi, "Porous silicon-based rugate filters," Appl. Optics **44**, 5415 (2005).

[9] M.-L. Lin, Y.-C. Lin, K.-H. Wu, and C.-P. Huang, "Preparation of oxidized nano-porous-silicon thin films for ultra-violet optical-sensing applications," Thin Solid Films **529**, 275 (2013).

[10] I. Suemune, N. Noguchi, and M. Yamanishi, "Photoirradiation Effect on Photoluminescence from anodized Porous silicons and luminesce Mechanism," Jpn. J. Appl. Phys. **31**, L494 (1992).

[11] L. A. Balagurov, S. C. Bayliss, S. Y. Andrushin, A. F. Orlov, B. Unal, D. G. Yarkin, and E. A. Petrova, "Metal/PS/c-Si photodetectors based on unoxidized and oxidized porous silicon," Solid State Electron. **45**, 1607 (2001).

[12] M. K. Lee, Y. H. Wang, and C. H. Chu, "Characterization of porous silicon photovoltaic devices through rapid thermal oxidation, rapid thermal annealing and HF-dipping processes," Sol. Energy Mater. & Sol Cells **59**, 59 (1999).

[13] L. Pavesi, "Porous silicon dielectric multilayers and microcavities," Riv. Nuovo Cimento **20**, 1 (1997).

[14] B. Gelloz, A. Kojima, and N. Koshida, "Stabilization and operation of porous silicon photonic structures from near-ultraviolet to near-infrared using high-pressure water vapor annealing," Thin Solid Films **518**, 3276 (2010).

[15] V. Torres, R. J. Martín, S. Manotas, F. Agullo, and J. M. Martínez, "Desarrollo de filtros interferenciales para emisores fotoluminicentes basados en Silicio Poroso," Bol. Soc. Esp. Ceram. V. **43**, 506 (2004).

[16] N. Khosida, A. Kojima, and Y. Nakajima, "Multifunctional properties of nanocrystalline porous silicon as a quantum-confined material," Mater. Sci. Eng. C **19**, 285 (2002).

[17] D. Brumhead, L. T. Canham, D. M. Seekings, and P. J. Tufton, "Gravimetric Analysis Of Pore Nucleation And Propagation In Anodised Silicon," Electrochim. Acta **38**, 191 (1993).

[18] W. M. Merrill, R. E. Diaz, M. M. Lore, M. C. Squires, and N. G. Alexopoulos, "Effective Medium Theories for Artificial Materials Composed of Multiple Sizes of Spherical Inclusions in a Host Continuum," IEEE Conf. Publ. **47**, 1 (1999).

[19] H. Münder, M. G. Berger, S. Frohnhoff, M. Thonissen, and H. Luth, "A non-destructive study of the microscopic structure of porous Si," J. Lumin. **57**, 5 (1993).

[20] P. Kumar, P. Lemmens, M. Ghosh, F. Ludwig, and M. Schilling, "Effect of HF Concentration on Physical and Electronic Properties of Electrochemically Formed Nanoporous Silicon," J. Nanomater. **2009**, 728957 (2009).

[21] V. Dzimbeg-Malcic, Z. Barbaric-Mikocevic, and K. Itric, "Kubelka-Munk Theory In Describing Optical Properties Of Paper," TEH VJESN **18**, 117 (2011).

[22] M. Krüger, S. Hilbrich, M. Thönissen, D. Scheyen, W. Theiß, and H. Lüth, "Suppression of ageing effects in porous silicon interference filters," Opt. Commun. **146**, 309 (1998).

[23] J. J. Yon, K. Barla, R. Herino, and G. Bomchil, "The kinetics and mechanism of oxide layer formation from porous silicon formed on p-Si subtrates," J. Appl. Phys. **62**, 1042 (1987).

[24] S. M. Sze, *Semiconductor Devices Physics and Technology* (2nd edition, Wiley, New York, 2002).

[25] J. E. Lugo, H. A. Lopez, S. Chan, and P. M. Fauchet, "Porous silicon multilayer structures: A photonic band gap analysis," J. Appl. Phys. **91**, 4966 (2002).

[26] M. S. Salem, M. J. Sailor, F. A. Harraz, T. Sakka, and Y. H.Ogata, "Electrochemical stabilization of porous silicon multilayers for sensing various chemical compounds," J. Appl. Phys. **100**, 83520 (2006).

[27] C. Pacholski, "Photonic Crystal Sensors Based on Porous Silicon," Sensors. **13**, 4694 (2013).

[28] J. Charrier, P. Pirasteh, Y.G. Boucher, and M. Gadonna, "Bragg reflector formed on oxidised porous silicon," Phys. Status Solidi C **2**, 3227 (2012).

[29] B. Sahaa, M. Sharmaa, A. Sarmaa, A. Rathb, P. V. Satyamb, P. Chakrabortya, and M. K. Sanyal, "Surface and interfacial structural characterization of MBE grown Si/Ge multilayers," Appl. Surf. Sci. **256**, 547 (2009).

[30] E. D. Palik (ed.), *Handbook of optical constants of solids* (Academic Press Inc., Washington DC, 1985).

[31] E. V. Astrova, V. B. Voronkov, A. D. Remenyuk, V. B. Shuman, and V. A. Tolmachev, "Variation of the parameters and composition of thin films of porous silicon as a result of oxidation: ellipsometric studies," Semiconductors **33**, 1149 (1999).

[32] A. Morales, E. Mora, and U. Pal, "Use of diffuse reflectance spectroscopy for optical characterization of un-supported nanostructures," Rev. Mex. Fis. **53**, 18 (2007).